Neuron, Volume *82*

Supplemental Information

Sleep and Movement Differentiates Actions of Two Types of Somatostatin-Expressing GABAergic Interneuron in Rat Hippocampus

Linda Katona, Damien Lapray, Tim J. Viney, Abderrahim Oulhaj, Zsolt Borhegyi, Benjamin R. Micklem, Thomas Klausberger, and Peter Somogyi

1. Supplemental Figures

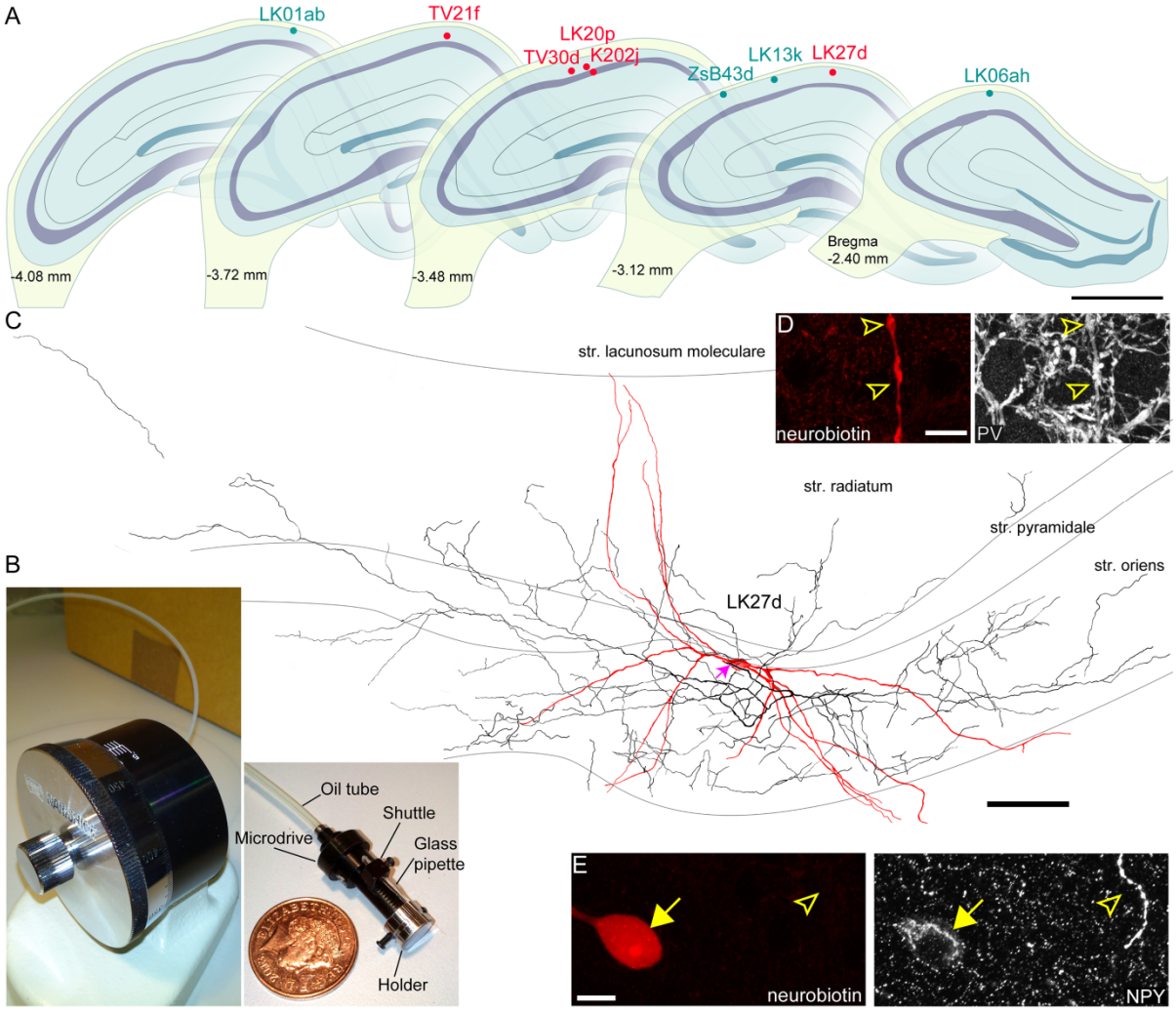

Figure S1. ***In vivo*** **extracellular recording and neurobiotin-labelling of single interneurons in freely moving rats and their positions in the hippocampus, related to Figures 1 and 2 and Experimental Procedures.** (A) Recording locations of labelled bistratified (red, n=5) and O-LM (blue, n=4) cells in CA1**.** Individual cell body locations in strata oriens and pyramidale are shown in schematic coronal sections from rostral to caudal direction, from left to right of the right hemisphere. Dark shaded bands show the pyramidal cell layer and the granule cell layer (blue) in the dentate gyrus. Scale bar, 1 mm. (B) Hydraulic (Narishige) microdrive *(right)* and manual manipulator *(left)*. *Right,* the metal holder is cemented to the rat's skull and

the microdrive is secured inside with screws. The shuttle holding the glass pipette is advanced by moving the manipulator connected via the oil tube. (C) Reconstruction of the soma, complete dendritic tree (red, n=9 ~70 μm thick sections) and representative part of the axon (black, 3 out of 20 70-μm-thick sections; axonal origin, magenta arrow) of a bistratified cell with a soma horizontally aligned with the pyramidal layer. Note the heavy axonal innervation of stratum oriens, but collaterals also entered stratum radiatum to a lower extent. (D) A tested dendrite (arrowheads) was immunopositive for PV (maximum intensity projection, z-stack, height 3.1 μm). (E) The cell body (arrow) and a neighbouring non-labelled axon (arrowhead) were immunopositive for NPY (maximum intensity projection, z-stack, height 3.9 μm). Scale bars, C 100 μm; D,E 10 μm.

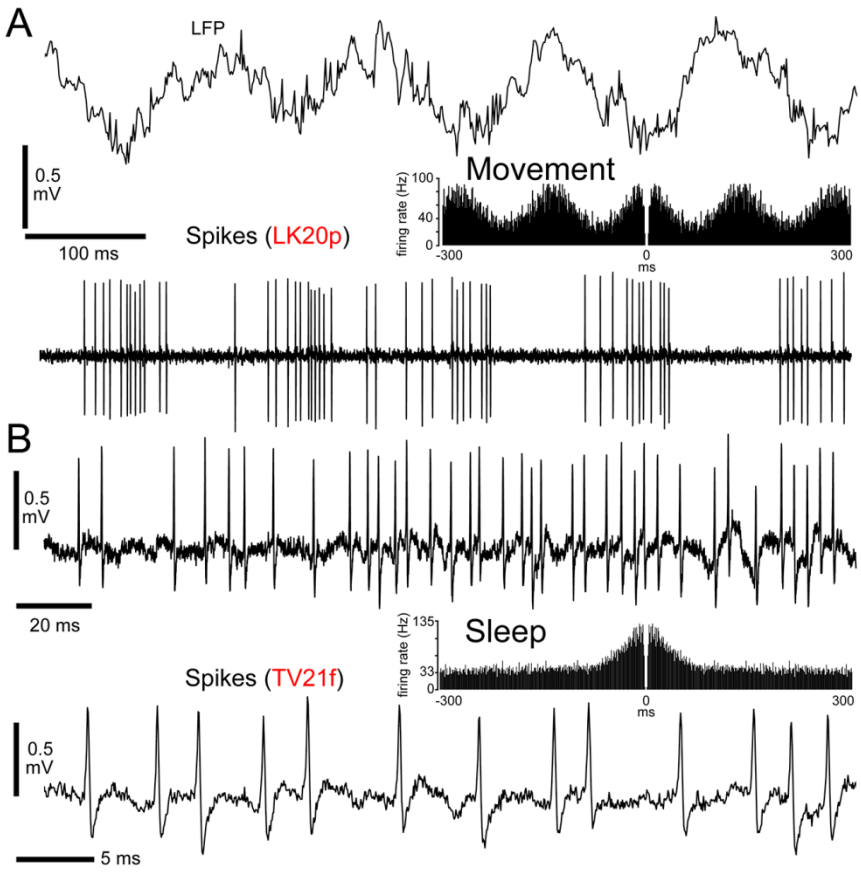

Figure S2. Firing patterns of bistratified cells during movement and sleep demonstrating short inter-spike intervals, related to Figures 1 and 3. (A) Spike train of a bistratified cell during movement. Note preferential timing of most spikes around the trough of the theta-oscillatory LFP (band-pass filtered 0.3-500 Hz). *Inset*, autocorrelogram of the interneuron. Note refractory period (1 ms time bins). (B) *Top*, spike train of a bistratified cell during sleep (band-pass filtered 0.8-5 kHz). *Bottom*, spike train at higher temporal resolution revealing uniform spike shapes. *Inset*, autocorrelogram of the interneuron. Note refractory period (1 ms time bins).

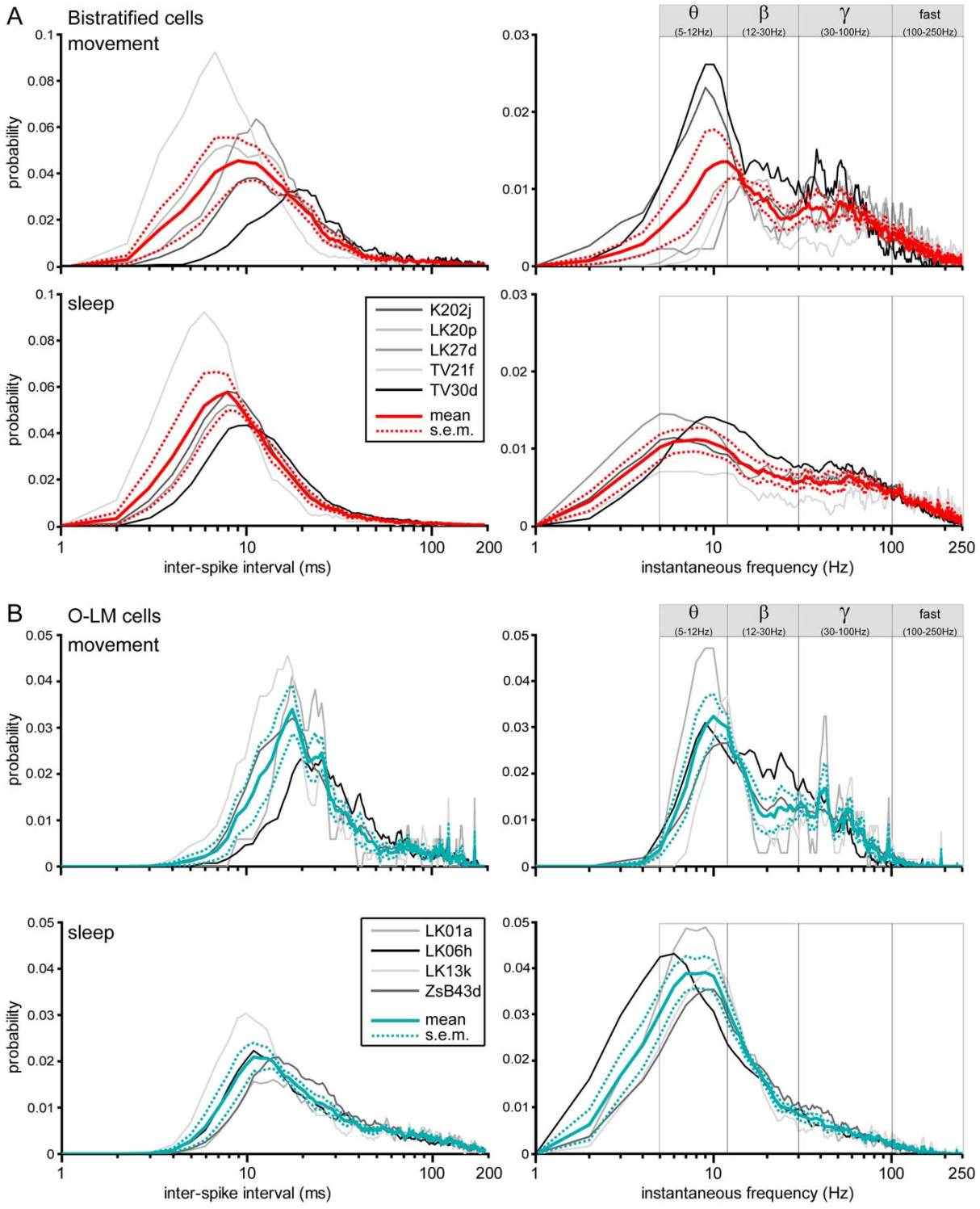

Figure S3. Individual inter-spike interval (ISI) and instantaneous frequency (IF) distributions of bistratified and O-LM cells, related to Figure 3. (A) *Left,* ISI distributions (mean ± s.e.m., solid and dashed lines) from all bistratified cells (individual cells, shades of grey; mean red) were calculated during sleep (*top*, n=4

cells) and movement (*bottom*, n=5 cells). Individual ISI distributions resembled each other more during sleep than during movement; TV21f had shorter ISIs than the other bistratified cells. *Right*, corresponding IF distributions across frequency ranges. (B) *Left*, ISI distributions (mean ± s.e.m., solid and dashed lines) from all O-LM cells (individual cells, shades of grey; mean blue) were calculated during sleep (*top*, n=4 cells) and movement (*bottom*, n=4 cells). Distributions were more similar during sleep than movement. Right, corresponding IF distributions. Note logarithmic time and frequency scales limited to 200 ms and 250 Hz, respectively.

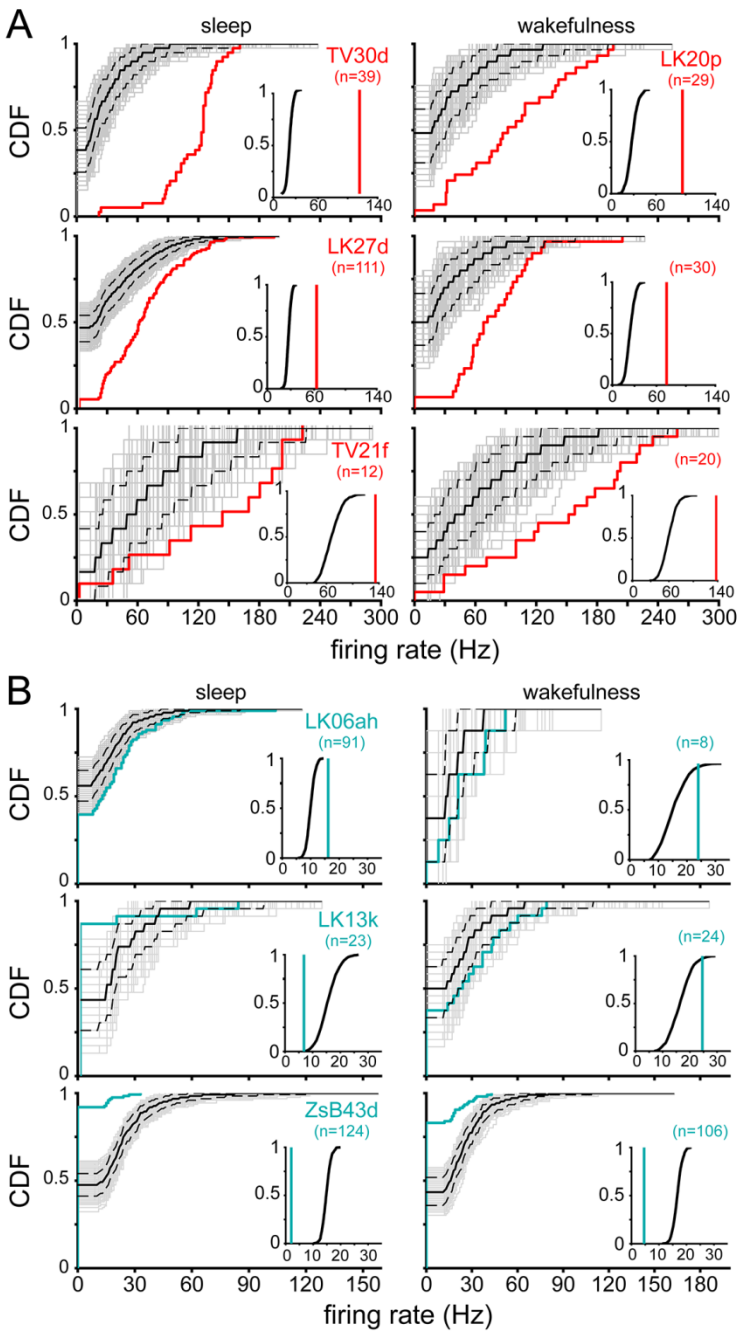

Figure S4. SWR-related firing rate distributions of bistratified and O-LM cells, during sleep and wakefulness, related to Figure 5. Bistratified cells (A) were activated by SWRs in all behavioural states (LK20p, no sleep period and TV30d no wakefulness recorded). The distribution of measured firing rates per individual SWRs are displayed as CDFs. For bistratified cells, the measured distributions (red) were significantly different from the medians (black) of the surrogate sets (2-sample KS-tests, n=4 cells in total, $p<0.05$ for all cells), and the right shift demonstrates an increase over the full range of firing rates. *Insets*, comparison of mean SWR-related firing rate (red lines), for each cell, with the distribution of surrogate mean rates (black lines). Bistratified cells (red) were strongly activated by SWRs, their measured mean rates were between 2 to 6 times higher than the means resulting from the surrogate distributions ($p<0.05$ for *sleep*; $p<0.05$ for *wakefulness*; relative to the CDFs for all four cells). O-LM cells (B)

changed their firing rates significantly during SWRs (2-sample KS-tests, n=3 cells in total, $p<0.05$, for all cells). The shift to the left or right of the measured CDFs (blue) relative to the median of the surrogate CDFs (grey) over the full or part of the surrogate firing rate range indicates decreased or increased firing of O-LM cells, respectively. Surrogate sets of 1000 firing rate-distributions (grey; median, solid black line; 95% confidence intervals, broken lines). *Insets*, comparison of mean SWR-related firing rate (blue lines), for each cell with the distribution of surrogate mean SWR-related rates (black lines). During *sleep*, the mean rates of LK13k and ZsB43d were decreased ($p=0.004$ for LK13k, $p=0$ for ZsB43d, probabilities given by CDFs) and the rate of LK06ah was increased ($p=0$, probability given by CDF). For cells LK06ah and LK13k in the *awake* condition, the measured rates were higher than those expected from the surrogate sets. *Insets*, comparison of mean SWR-related firing rates (blue lines) with the distribution of surrogate mean SWR-related rates (black lines). The rate of ZsB43d was decreased ($p=0$, relative to the CDF) and the rates of LK06ah and LK13k were increased ($p=0.01$ for LK06ah; $p=0.009$ for LK13k; probabilities given by CDFs) during SWRs. Note the differences in X axis scales between bistratified and O-LM cells in the insets.

Table S1. Statistical comparison of firing rates, bursting probability and spike counts of bistratified, O-LM and PV+ basket cells, related to Results.

			One-way ANOVA		Kruskal Wallis test	
Measure	**Comparison between**	**Condition**	**F**	**p**	**χ^2**	**p**
Firing rates	bistratified, O-LM and PV+ basket cells	movement	2.02 (2,11)	0.1788	2.5657	0.2772
		sleep	6.68 (2,10)	0.0144	7.9813	0.0185
		quiet wakefulness	2.28 (2,11)	0.1485	3.9057	0.1419
		theta oscillations	3.75 (2,11)	0.0572	4.7057	0.0951
		SWRs	23.73 (2,11)	0.0001	8.4629	0.0145
		LOSC	23.09 (2,10)	0.0002	8.6044	0.0135
Bursting probability	bistratified and O-LM cells	theta cycles	7.41 (1,7)	0.0297	6	0.0143
		SWRs	27.38 (1,7)	0.0012	6	0.0143
Mean number of spikes	bistratified and O-LM cells	sleep-SWRs	49.59 (1,6)	0.0004	5.3333	0.0209
		awake-SWRs	23.76 (1,6)	0.0028	5.3333	0.0209
	sleep-SWRs and awake-SWRs	bistratified cells	0.33 (1,6)	0.5864	0.3333	0.5637
		O-LM cells	1.36 (1,6)	0.2884	1.3333	0.2482

Table S2. Antibody information, related to Experimental Procedures.

Molecule	Host species	Internal ref No.	Dilution	Stock protein concentration (µg/ml)	Source	Source code
calbindin (CB)	rabbit	989	1:5000	antiserum	Swant, Bellinzona, Switzerland **(www.swant.com)**	CB-38 (lot 5.5)
tyrosine-protein kinase receptor (ErbB4)	mouse	1353	1:1000	200	Thermo Fisher Scientific, Kalamazoo, MI, USA **(www.labvision.com)**	MS-270-P, clone H4.77.16
extracellular leucine-rich repeat fibronectin containing protein-2 (Elfn 2)	rabbit	1432	1:500		Sigma-Aldrich, St. Louis, MO, USA **(www.sigma-aldrich.com)**	HPA000781
multizinc finger protein (Fog-2) M-247	rabbit	1369	1:200	200	Santa Cruz Biotechnology Inc., Santa Cruz,CA, USA **(www.scbt.com)**	sc-10755
metabotropic glutamate receptor-1 alpha subunit (mGluR1a)	goat	1266	1:750	1220	Prof. M. Watanabe, FRONTIER INSTITUTE Co. Ltd, Hokkaido, Japan	(Kind gift)
metabotropic glutamate receptor-1 alpha subunit (mGluR1a)	guinea pig	1267	1:500 1:1000 1:2000	660	Prof. M. Watanabe, FRONTIER INSTITUTE Co. Ltd, Hokkaido, Japan	(Kind gift)
metabotropic glutamate receptor-7 alpha subunit (mGluR7a)	rabbit	960	1:1000 1:2000	500	Prof. R. Shigemoto, Division of Cerebral Structure, Nat. Inst. Physiol. Sci, Okazaki, Japan	(Kind gift)
parvalbumin (PV)	goat	1258	1:1000 1:2000	antiserum	Swant, Bellinzona, Switzerland **(www.swant.com)**	PVG-214 (lot 3.6)
parvalbumin (PV)	guinea pig	1310	1:5000	antiserum	Synaptic Systems, Entwicklung und Produktion mbH, Goettingen, Germany **(www.sysy.com)**	195 004 (lot5)
parvalbumin (PV)	mouse	922	1:5000	antiserum	Swant, Bellinzona, Switzerland **(www.swant.com)**	235 (lot 10-11 F)
special AT-rich sequence-binding protein-1 (Satb1) N-14	goat	1394	1:200	200	Santa Cruz Biotechnology Inc., Santa Cruz,CA, USA **(www.scbt.com)**	sc-5989
special AT-rich sequence-binding protein-2 (Satb2) SATBA4B10	mouse	1341	1:100	100	Abcam, Cambridge, UK **(www.abcam.com)**	ab51502
special AT-rich sequence-binding protein-1 (Satb1) N-14	rabbit	1393	1:1000	1000	Abcam, Cambridge, UK **(www.abcam.com)**	ab70004
somatostatin (SM)	mouse	1276	1:200 1:400 1:500	140	GeneTex Inc., Irvine, CA, USA **(www.genetex.com)**	GTX71935 (clone SOM-018)
somatostatin (SM)	rat	815	1:500	1000	EMD Millipore Corporation, Billerica, MA, USA **(www.millipore.com)**	MAB354
neuropeptide Y (NPY)	rabbit	1011	1:5000	antiserum	ImmunoStar Inc.(DiaSorin), Hudson, WI, USA **(www.immunostar.com)**	22940 (lot 208001)

Molecule (repeated)	Host species	Epitope, amino acid residues	Antibody specificity information	Notes
calbindin (CB)	rabbit	polyclonal, recombinant rat calbindin D-28k	Knock out test in mouse: (Airaksinen et al., 1997); characterisation in rat hippocampus: (Sloviter, 1989).	
tyrosine-protein kinase receptor (ErbB4)	mouse	monoclonal, extracellular fragment, recombinant human c-erbB4/HER-4 oncoprotein	Generation, knock out tests, western blot band as expected: (Chen et al., 1996; Neddens et al., 2011; Vullhorst et al., 2009).	Cortical GABA circuit development controlled by ErbB4 signalling (Fazzari et al., 2010).
extracellular leucine-rich repeat fibronectin containing protein-2 (Elfn 2)	rabbit	polyclonal, affinity isolated, human ELFN2, recombinant protein epitope signature tag	Protein array and western blot tests: (Sylwestrak and Ghosh, 2012); developed and validated by the Human Protein Atlas project.	Labels interneurons via cross-reactivity with Elfn1.
multizinc finger protein (Fog-2) M-247	rabbit	polyclonal, epitope aa880-1126 mapping at the C-terminus of FOG-2 of mouse origin	Western blot by the company (Dale et al., 2007; Roche et al., 2008).	
metabotropic glutamate receptor-1 alpha subunit (mGluR1a)	goat		Personal communication with Prof. M. Watanabe.	In some interneurons it labels a reticular pattern instead of labelling the plasma membrane.
metabotropic glutamate receptor-1 alpha subunit (mGluR1a)	guinea pig	affinity purified	(Nakamura et al., 2004)	In some interneurons it labels a reticular pattern instead of labelling the plasma membrane.
metabotropic glutamate receptor-7 alpha subunit (mGluR7a)	rabbit	rat mGluR7 affinity purified, aa874-915	(Klausberger et al., 2005; Shigemoto et al., 1997; Shigemoto et al., 1996)	
parvalbumin (PV)	goat	polyclonal, rat muscle PV	Knock out tests in mouse: (Schwaller et al., 1999), Swant; western blot on rodent brain homogenate, single ~12 kDa band labelled (p. comm. E. Celio): (Constantinople et al., 2009).	
parvalbumin (PV)	guinea pig	polyclonal, recombinant full length rat PV	Western blot, abolished by pre-absorption with recombinant PV; knockout test in mouse:(Schwaller et al., 1999); same labelling with antibodies from: Synaptic Systems, rabbit 195 002, Swant, monoclonal 235; rat hippocampus: (Kosaka et al., 1987; Sloviter, 1989).	
parvalbumin (PV)	mouse	monoclonal, purified carp muscle PV	Knockout tests: in mouse (Schwaller et al., 1999); similar to other PV antibodies; characterization: (Celio et al., 1988).	
special AT-rich sequence-binding protein-1 (Satb1) N-14	goat	polyclonal, N-terminus, human SATB1	Knockout test in mouse: (Balamotis et al., 2012); mouse cortex: (Huang et al., 2011); same labelling as rabbit antibody ab70004.	Labels in addition SATB2-expressing nuclei in CA1 when used at 1:100 dilution. Weakly labels hilar neuron nuclei.
special AT-rich sequence-binding protein-2 (Satb2) SATBA4B10	mouse	monoclonal, recombinant fragment C-terminal, human SATB2.	Knockout tests in mouse: (Britanova et al., 2005; Britanova et al., 2008; Britanova et al., 2006; Dobreva et al., 2006); adult mouse brain: (Nielsen et al., 2010); same labelling as rabbit antibody ab34735 with additional signal for SATB1.	Labels pyramidal cells and a subpopulation of interneurons in CA1, consistent with the combination of specific SATB2 and SATB1 antibodies.
special AT-rich sequence-binding protein-1 (Satb1) N-14	rabbit	polyclonal, 18 aa near N-terminus, human SATB1	Knockout test in mouse: (Balamotis et al., 2012); mouse cortex: (Huang et al., 2011); no singal for knockout for a similar rabbit antibody; original rabbit antibody: (Dickinson et al., 1992); western blot in mouse, different band than SATB2 at P1; colocalization with NeuN, neuron specific.	Labels interneurons exclusively in hippocampus.
somatostatin (SM)	mouse	monoclonal, conjugated to protein carrier, human SOM	Rat antibody test: (Kubota et al., 2011); labelling pattern same as with rat antibody Chemicon MAB364; no signal in preabsorption test for rat antibody; mouse hippocampus using rat antibody: (Jinno and Kosaka, 2000).	Labels dendrites and axon stronger than other SOM antibodies.
somatostatin (SM)	rat	monoclonal, synthetic 1-14 cyclic SOM conjugated to bovine thyroglobulin using carbodiimide	Same labelling as other antibodies: (Kubota et al., 2011).	
neuropeptide Y (NPY)	rabbit	polyclonal, synthetic porcine NPY conjugated to methylated bovine serum albumin.	Antibody generation and characterization: (Allen et al., 1983); absorption-tested by manufacturer to 6 other peptides, no cross-reactivity observed; labelling as with other antibodies.	Strong immunoreactivity observed in subpopulations of hippocampal interneurons, no significant background.

Table S3. Point estimates of ISI distributions of bistratified and O-LM cells, related to Figure 3 and 4 and Supplemental Figure S3.

		Median ± interquartile range of ISI (ms)		
Cell type	**Cell**	**Movement**	**Sleep**	**Quiet wakefulness**
Bistratified cells	K202j	20.4 ± 37.3	13.2 ± 22.3	15.9 ± 31.1
	LK20p	12.6 ± 17.3	NA ± NA	12.9 ± 21.1
	LK27d	13.3 ± 14.3	15.0 ± 26.9	13.5 ± 16.8
	TV21f	7.7 ± 10.2	7.7 ± 10.9	7.3 ± 9.1
	TV30d	25.8 ± 43.4	17.4 ± 29.8	22.8 ± 42.5
O-LM cells	LK01ab	26.0 ± 66.4	65.6 ± 101.5	42.7 ± 66.3
	LK06ah	39.2 ± 44.6	54.8 ± 119.6	41.8 ± 60.2
	LK13k	22.5 ± 38.3	45.5 ± 87.8	26.2 ± 45.1
	ZsB43d	27.6 ± 43.7	44.4 ± 76.5	42.1 ± 57.5

Cell type	**Cell**	**Theta**	**SWRs**	**LOSC**
Bistratified cells	K202j	22.4 ± 36.3	6.4 ± 3.7	24.1 ± 73.2
	LK20p	13.2 ± 19.4	6.2 ± 4.3	20.9 ± 21.9
	LK27d	13.4 ± 15.4	8.9 ± 8.2	14.1 ± 19.8
	TV21f	7.6 ± 9.9	4.9 ± 2.9	NA ± NA
	TV30d	23.1 ± 46.7	6.7 ± 3.4	20.4 ± 46.4
O-LM cells	LK01ab	36.2 ± 66.2	15.0 ± 19.7	44.5 ± 54.5
	LK06ah	38.9 ± 54.3	14.9 ± 19.3	45.8 ± 53.0
	LK13k	23.3 ± 47.6	7.1 ± 4.1	30.0 ± 45.7
	ZsB43d	38.2 ± 53.8	20.1 ± 5.4	43.5 ± 60.1

2. Supplemental Experimental Procedures

Experimental subjects

Animals were housed in groups of 2–4 per cage in Oxford (8 rats; 19–21C°; 55% humidity; reverse light/dark cycle, lights on from 8pm–8am) or Vienna (1 rat; diurnal cycle, lights on from 6am–6pm). One to 7 days before the protocol started, rats were housed in a cage on their own with *ad libitum* access to food pellets and water. The rat in Vienna received chocolate chip rewards given during some recording sessions.

Microdrive, recording and reference electrodes

In short, we attached a cylindrical microdrive holder above the left parietal cortex using dental acrylic (Refobacin R, Biomet). A main connector was placed above the frontal part of the skull, supported by five stainless steel screws. EEG and reference-ground signals were fed into this head stage from one screw above the right prefrontal cortex (bregma -4 mm rostro-caudal, bregma +2 mm medio-lateral) and another above the cerebellum, respectively. Following recovery of a minimum of three days, the animal was anaesthetised, and after a craniotomy either a single wire electrode (50 μm tungsten, California Fine Wire; n=5 rats) fixed on the skull or movable by a miniature drive (Haiss et al., 2010) or a microdrive movable tetrode (n=4 rats) (Neuronelektrod Kft., Budapest, Hungary) was lowered into the right hippocampus or cortex. A layer of silicone (Kwik-Sil, World Precision Instruments) was used to protect the cortical surface between recordings.

In vivo behavioural recordings and juxtacellular neurobiotin-labelling in freely moving rats and data acquisition

Rats were anaesthetised briefly by isoflurane and a miniature preamplifier (NPI Electronic), two LED arrays and an accelerometer (Supertech Instruments; n=5

rats) were connected to the head stage. A glass electrode filled with neurobiotin (1.5 or 3%, wt/vol, in 0.5 M NaCl) was advanced using a hydraulic (Narishige, Figure S1B) or piezoelectric (Kleindiek Nanotechnik) (Lee et al., 2006) microdrive. Recordings commenced 1h after recovery from anaesthesia in a darkened room using a recording arena (40 $\times$ 40 cm floor; 27 cm walls or 50 $\times$ 50 cm floor, 27 cm walls in Oxford; 40 $\times$ 60cm floor, 30 cm walls in Vienna) to which the rats were naive on the first day. The rats were followed on two video cameras, one infra-red sensitive for behavioural analysis and another one for position tracking (software courtesy of Dr. K. Allen). Recordings were performed for 1–12 days (4.9 $\pm$ 3.1 days) after duratomy. After recording a cell, the pipette was advanced towards the neuron and juxtacellular labelling was attempted (Pinault, 1996). When deemed successful, the pipette was retracted slightly and the neuron was left to recover from the entrainment. The animal was deeply anaesthetised and perfusion fixed 1–3 h later. When stable neurons were not found sessions were finished by removal of the recording setup and by covering the cortical surface with silicone between consecutive days.

Signals were amplified 1000x (BF-48DGX and DPA-2FS, NPI Electronic) and digitised at 1 or 20 kHz (Power1401 A/D board, Cambridge Electronics Design). Measurements from the glass electrode were online band-pass filtered according to three different frequency ranges (0.3 Hz –10 kHz, wide-band; 0.3–500 Hz, LFP; 0.8–5 kHz, action potentials). Signals from the hippocampal/cortical electrodes were wide-band filtered. Elimination of 50 Hz noise without phase-shift was provided by Hum Bugs (Quest Scientific Instruments). Accelerometer measurements were digitised at 1 or 20 kHz. Acquisition of all signals, except tracking, went in parallel using Spike2 software (v7.01, Cambridge Electronics Design).

Electrophysiological data analyses

For each interneuron, we computed the theta phases of the recorded spikes. We determined whether the cell was theta modulated using Rayleigh's method (Zar, 1999) and if the theta phases resulted in a non-uniform distribution around the theta cycle. Using normalised vector addition, we calculated the cell's mean phase angle and the depth of the cell's theta modulation. Data was averaged across individual cells of the same type. For the quantitative comparison of distinct cell types we used two-sample permutation tests (Good, 2000).

Recorded spike trains were segmented according to behavioural and oscillatory network states and analysed one by one. For each interneuron, the periods between two consecutive action potentials (ISI) have been measured and their distributions analysed. The ISI distributions of individual cells of a given type were averaged and the resulting mean $\pm$ s.e.m. was considered as the representative ISI distribution for the cell type during a given state. Additionally, we calculated point estimates (median $\pm$ interquartile range) for the individual ISI distributions per cell and per state (Table S3).

Neuronal 3D reconstructions

Neurons were digitally reconstructed in 3D from resin-embedded, osmium-treated sections reacted for HRP using Neurolucida (MBF Bioscience), a Nikon Eclipse 80i transmitted light microscope and Lucivid microdisplay (MBF Bioscience) in continuous mode using a VC Plan Apo 100x/1.4 oil immersion objective.

Antibody information

Secondary antibodies conjugated to Alexa488 and Alexa405 fluorophores were purchased from Invitrogen. Secondary antibodies conjugated to Cy3, Cy5, DyLight405, DyLight488, DyLight594 and DyLight649 fluorophores were purchased from Stratech.

3. Supplemental References

Airaksinen, M.S., Eilers, J., Garaschuk, O., Thoenen, H., Konnerth, A., and Meyer, M. (1997). Ataxia and altered dendritic calcium signaling in mice carrying a targeted null mutation of the calbindin D28k gene. Proc. Natl. Acad. Sci. USA 94, 1488-1493.

Allen, Y.S., Adrian, T.E., Allen, J.M., Tatemoto, K., Crow, T.J., Bloom, S.R., and Polak, J.M. (1983). Neuropeptide Y distribution in the rat brain. Science 221, 877-879.

Balamotis, M.A., Tamberg, N., Woo, Y.J., Li, J., Davy, B., Kohwi-Shigematsu, T., and Kohwi, Y. (2012). Satb1 ablation alters temporal expression of immediate early genes and reduces dendritic spine density during postnatal brain development. Mol. Cell Biol. 32, 333-347.

Britanova, O., Akopov, S., Lukyanov, S., Gruss, P., and Tarabykin, V. (2005). Novel transcription factor Satb2 interacts with matrix attachment region DNA elements in a tissue-specific manner and demonstrates cell-type-dependent expression in the developing mouse CNS. Eur. J. Neurosci. 21, 658-668.

Britanova, O., de Juan Romero, C., Cheung, A., Kwan, K.Y., Schwark, M., Gyorgy, A., Vogel, T., Akopov, S., Mitkovski, M., Agoston, D.*, et al.* (2008). Satb2 is a postmitotic determinant for upper-layer neuron specification in the neocortex. Neuron 57, 378-392.

Britanova, O., Depew, M.J., Schwark, M., Thomas, B.L., Miletich, I., Sharpe, P., and Tarabykin, V. (2006). Satb2 haploinsufficiency phenocopies 2q32-q33 deletions, whereas loss suggests a fundamental role in the coordination of jaw development. Am. J. Hum. Genet. 79, 668-678.

Celio, M.R., Baier, W., Schärer, L., De Viragh, P.A., and Gerday, C. (1988). Monoclonal antibodies directed against the calcium binding protein parvalbumin. Cell Calcium 9, 81-86.

Chen, X., Levkowitz, G., Tzahar, E., Karunagaran, D., Lavi, S., Ben-Baruch, N., Leitner, O., Ratzkin, B.J., Bacus, S.S., and Yarden, Y. (1996). An immunological approach reveals biological differences between the two NDF/Heregulin receptors, ErbB-3 and ErbB-4. J. Biol. Chem. 271, 7620-7629.

Constantinople, C.M., Disney, A.A., Maffie, J., Rudy, B., and Hawken, M.J. (2009). Quantitative analysis of neurons with Kv3 potassium channel subunits, Kv3.1b and Kv3.2, in macaque primary visual cortex. J. Comp. Neurol. 516, 291-311.

Dale, R.M., Remo, B.F., and Svensson, E.C. (2007). An alternative transcript of the FOG-2 gene encodes a FOG-2 isoform lacking the FOG repression motif. Biochem. Biophys. Res. Commun. 357, 683-687.

Dickinson, L.A., Joh, T., Kohwi, Y., and Kohwi-Shigematsu, T. (1992). A tissue-specific MARSAR DNA-binding protein with unusual binding site recognition. Cell 70, 631-645.

Dobreva, G., Chahrour, M., Dautzenberg, M., Chirivella, L., Kanzler, B., Fariñas, I., Karsenty, G., and Grosschedl, R. (2006). SATB2 is a multifunctional determinant of craniofacial patterning and osteoblast differentiation. Cell 125, 971-986.

Fazzari, P., Paternain, A.V., Valiente, M., Pla, R., Lujan, R., Lloyd, K., Lerma, J., Marin, O., and Rico, B. (2010). Control of cortical GABA circuitry development by Nrg1 and ErbB4 signalling. Nature 464, 1376-1380.

Good, P. (2000). Permutation tests : a practical guide to resampling methods for testing hypotheses (New York: Springer).

Haiss, F., Butovas, S., and Schwarz, C. (2010). A miniaturized chronic microelectrode drive for awake behaving head restrained mice and rats. J. Neurosci. Methods 187, 67-72.

Huang, Y., Zhang, L., Song, N.-N., Hu, Z.-L., Chen, J.-Y., and Ding, Y.-Q. (2011). Distribution of Satb1 in the central nervous system of adult mice. Neurosci. Res. 71, 12-21.

Jinno, S., and Kosaka, T. (2000). Colocalization of parvalbumin and somatostatin-like immunoreactivity in the mouse hippocampus: Quantitative analysis with optical disector. J. Comp. Neurol. 428, 377-388.

Klausberger, T., Marton, L.F., O'Neill, J., Huck, J.H.J., Dalezios, Y., Fuentealba, P., Suen, W.Y., Papp, E., Kaneko, T., Watanabe, M.*, et al.* (2005). Complementary roles of cholecystokinin- and parvalbumin-expressing GABAergic neurons in hippocampal network oscillations. J. Neurosci. 25, 9782-9793.

Kosaka, T., Katsumaru, H., Hama, K., Wu, J.-Y., and Heizmann, C.W. (1987). GABAergic neurons containing the Ca2+-binding protein parvalbumin in the rat hippocampus and dentate gyrus. Brain Res. 419, 119-130.

Kubota, Y., Shigematsu, N., Karube, F., Sekigawa, A., Kato, S., Yamaguchi, N., Hirai, Y., Morishima, M., and Kawaguchi, Y. (2011). Selective coexpression of multiple chemical markers defines discrete populations of neocortical GABAergic neurons. Cereb. Cortex 21, 1803-1817.

Lee, A.K., Manns, I.D., Sakmann, B., and Brecht, M. (2006). Whole-cell recordings in freely moving rats. Neuron 51, 399-407.

Nakamura, M., Sato, K., Fukaya, M., Araishi, K., Aiba, A., Kano, M., and Watanabe, M. (2004). Signaling complex formation of phospholipase Cβ4 with metabotropic glutamate receptor type 1α and 1,4,5-trisphosphate receptor at the perisynapse and endoplasmic reticulum in the mouse brain. Eur. J. Neurosci. 20, 2929-2944.

Neddens, J., Fish, K.N., Tricoire, L., Vullhorst, D., Shamir, A., Chung, W., Lewis, D.A., McBain, C.J., and Buonanno, A. (2011). Conserved interneuron-specific ErbB4 expression in frontal cortex of rodents, monkeys, and humans: Implications for schizophrenia. Biol. Psychiatry 70, 636-645.

Nielsen, J.V., Blom, J.B., Noraberg, J., and Jensen, N.A. (2010). Zbtb20-induced CA1 pyramidal neuron development and area enlargement in the cerebral midline cortex of mice. Cereb. Cortex 20, 1904-1914.

Pinault, D. (1996). A novel single-cell staining procedure performed in vivo under electrophysiological control: morpho-functional features of juxtacellularly labeled thalamic cells and other central neurons with biocytin or Neurobiotin. J. Neurosci. Methods 65, 113-136.

Roche, A.E., Bassett, B.J., Samant, S.A., Hong, W., Blobel, G.A., and Svensson, E.C. (2008). The zinc finger and C-terminal domains of MTA proteins are required for FOG-2-mediated transcriptional repression via the NuRD complex. J. Mol. Cell. Cardiol. 44, 352-360.

Schwaller, B., Dick, J., Dhoot, G., Carroll, S., Vrbova, G., Nicotera, P., Pette, D., Wyss, A., Bluethmann, H., Hunziker, W., and Celio, M.R. (1999). Prolonged contraction-relaxation cycle of fast-twitch muscles in parvalbumin knockout mice. Am. J. Physiol. Cell Physiol. 276, C395-C403.

Shigemoto, R., Kinoshita, A., Wada, E., Nomura, S., Ohishi, H., Takada, M., Flor, P.J., Neki, A., Abe, T., Nakanishi, S., and Mizuno, N. (1997). Differential presynaptic localization of metabotropic glutamate receptor subtypes in the rat hippocampus. J. Neurosci. 17, 7503-7522.

Shigemoto, R., Kulik, A., Roberts, J.D.B., Ohishi, H., Nusser, Z., Kaneko, T., and Somogyi, P. (1996). Target-cell-specific concentration of a metabotropic glutamate receptor in the presynaptic active zone. Nature 381, 523-525.
Sloviter, R.S. (1989). Calcium-binding protein (calbindin-D28k) and parvalbumin immunocytochemistry: Localization in the rat hippocampus with specific reference to the selective vulnerability of hippocampal neurons to seizure activity. J. Comp. Neurol. 280, 183-196.
Sylwestrak, E.L., and Ghosh, A. (2012). Elfn1 regulates target-specific release probability at CA1-interneuron synapses. Science 338, 536-540.
Vullhorst, D., Neddens, J., Karavanova, I., Tricoire, L., Petralia, R.S., McBain, C.J., and Buonanno, A. (2009). Selective expression of ErbB4 in interneurons, but not pyramidal cells, of the rodent hippocampus. J. Neurosci. 29, 12255-12264.
Zar, J.H. (1999). Biostatistical analysis, 4 edn (Upper Saddler River: Prentice Hall).